Intersystem Crossing as Vibronically-Induced Phonon Emission and Absorption Processes: A Unified View of Nonradiative Transitions in a Molecule

Wataru Ota,[1,2] Motoyuki Uejima,[3] Naoki Haruta,[1,2] and Tohru Sato[1,2]

[1)]*Fukui Institute for Fundamental Chemistry, Kyoto University, Takano Nishibiraki-cho 34-4, Sakyo-ku, Kyoto 606-8103, Japan*

[2)]*Department of Molecular Engineering, Graduate School of Engineering, Kyoto University, Nishikyo-ku, Kyoto 615-8510, Japan*

[3)]*MOLFEX, Inc., Takano Nishibiraki-cho 34-4, Sakyo-ku, Kyoto 606-8103, Japan*

(*Electronic mail: tsato@scl.kyoto-u.ac.jp)

(Dated: 2 October 2023)

An analytical expression for the nonradiative rate constant is derived based on Fermi's golden rule within the mixed-spin crude adiabatic (CA) approximation. The mixed-spin CA basis is defined by a set of eigenstates for the electronic Hamiltonian that comprises the nonrelativistic electronic Hamiltonian and spin-orbit coupling clumped at the reference nuclear configuration. The mixed-spin basis differs from the pure-spin basis defined by a set of eigenstates for the nonrelativistic electronic Hamiltonian. The mixed-spin CA representation provides a unified view of the nonradiative transition; both internal conversion and intersystem crossing (ISC) are regarded as vibronically-induced phonon emission and absorption processes. The analytical expression enables us to determine important vibrational modes responsible for phonon emission/absorption (promoting modes) and accepting excitation energy (accepting modes) according to the selection rule of vibronic coupling. An advantage of the CA representation is that the spatial distribution of vibronic coupling is elucidated based on its density form, i.e., vibronic coupling density, which can be applied to theoretical molecular design with controlled nonradiative processes. The calculated ISC rate constant of tetracene reproduces the experimental result well.

I. INTRODUCTION

Nonradiative transitions between electronic states are classified into internal conversion (IC) and intersystem crossing (ISC), depending on whether the spin multiplicities before and after the transition are the same or different [1,2]. Two representations are well-known to treat nuclear motions in a molecule: Born-Oppenheimer (BO) and crude adiabatic (CA) representations [3,4]. In the BO representation, a vibronic wavefunction is expanded by the electronic basis that depends on the nuclear coordinates. In contrast, in the CA representation, a vibronic wavefunction is expanded by the electronic basis fixed at the reference nuclear configuration. Formulating the nonradiative rate constant using Fermi's golden rule is commonly based on the BO representation [2,5,6]. The perturbation to induce IC in the BO and CA representations is derivative coupling and vibronic coupling, respectively [3,4].

The perturbation for ISC changes depending on whether the electronic states are pure-spin or mixed-spin states, which are defined by the eigenstates of the zeroth-order electronic Hamiltonian that excludes or includes the spin-orbit (SO) coupling, respectively [7–17]. The currently most used representation to formulate the ISC rate constant is the pure-spin BO one. [18–22], In this case, ISC is induced by direct SO coupling at the first-order perturbation and SO coupling plus derivative coupling at the second-order perturbation. Historically, Siebrand et al. suggested employing the pure-spin BO representation to consider ISC between pure-spin states that are easy to associate with experimental observations [7–10]. In contrast, Azumi et al. suggested employing the mixed-spin BO representation, in which ISC is regarded as a nonradiative transition between mixed-spin states induced by derivative coupling at the first-order perturbation [11,12]. This representation allows a unified treatment of the nonradiative transitions because the driving force of IC and ISC becomes the same [13,14]. Note also that the mixed-spin basis has been widely used for phosphorescence rate expression; phosphorescence is a radiative transition between mixed-spin states induced by electron-photon coupling [18,23–25].

We previously derived an analytical expression for the IC rate constant based on Fermi's golden rule using the CA representation instead of the BO one [26]. IC can be interpreted as a phonon emission and absorption process, in analogy to a photon emission (fluorescence) and absorption process. This view clarifies the role of vibronic coupling in the IC process; vibrational modes are classified into promoting modes (responsible for phonon emission and absorption) and accepting modes (responsible for accepting excitation energy) according to the selection rule of vibronic

coupling. In addition, an advantage of the CA representation is that the origin of vibronic coupling can be elucidated by its density form, vibronic coupling density (VCD), which is utilized for rational molecular design [27–29]. The VCD concept has been applied to various fluorescent molecules to obtain chemical insights into the IC processes [30–33].

In this study, we derive an analytical expression for the nonradiative rate constant based on Fermi's golden rule using the mixed-spin CA representation, which can be applied to IC and ISC in a unified framework. All vibrational modes are considered on an equal footing in the rate expression. A mixed-spin state is written as a linear combination of pure-spin states, wherein the mixing coefficients between the pure-spin states are obtained by diagonalizing the electronic Hamiltonian represented by the pure-spin CA basis. The irreducible representation (irrep) of a double group [34–37] is employed, i.e., the irrep of a pure-spin state is expressed as that of spatial and spin parts separately, to clarify the ISC channel from the selection rule of SO coupling and vibronic coupling. The density of the final vibronic states weighted by the vibrational matrix element is evaluated in the time-correlation function formalism [38,39]. Tetracene, for which the ISC rate constant was experimentally [1,40,41] and theoretically investigated [42,43], is used as an illustrative example.

The paper is organized as follows: in Section 2, we derive an analytical expression for the ISC rate constant. Section 3 describes the computational details, and Section 4 provides the calculated results for the ISC rate constant and VCD of tetracene. Section 5 concludes this study.

II. THEORY

This section is organized as follows: in Section 2.1, we derive a general expression for the nonradiative rate constant based on Fermi's golden rule within the mixed-spin CA approximation. Section 2.2 defines the vibronic coupling constant (VCC) between mixed-spin states. In Section 2.3, we obtain the ISC rate constant using several assumptions and approximations. Section 2.4 provides an analytical expression for the nuclear part of the ISC rate constant. Section 2.5 defines the VCD for mixed-spin states.

A. Rate Constant of Nonradiative Transition within the Mixed-Spin Crude Adiabatic Approximation

A molecule with M nuclei and N electrons is considered. A set of electronic coordinates is denoted by $\mathbf{r} = (\mathbf{r}_1, \cdots, \mathbf{r}_i, \cdots, \mathbf{r}_N)$ with $\mathbf{r}_i = (x_i, y_i, z_i)$ in the Cartesian coordinates. A set of mass-weighted normal coordinates is denoted by $\mathbf{Q} = (Q_1, \cdots, Q_\alpha, \cdots, Q_{3M-5 \text{ or } 3M-6})$. Molecular deformation from a reference nuclear configuration is described by normal coordinates [27,44]. A vibronic Hamiltonian is given by[3]

$$\mathscr{H}(\mathbf{r},\mathbf{Q}) = \mathscr{T}_n(\mathbf{Q}) + \widetilde{\mathscr{H}_e}(\mathbf{r},\mathbf{Q}), \tag{1}$$

$$\widetilde{\mathscr{H}_e}(\mathbf{r},\mathbf{Q}) = \mathscr{H}_e(\mathbf{r},\mathbf{Q}) + \mathscr{H}_{\mathrm{SO}}(\mathbf{r},\mathbf{Q}), \tag{2}$$

where $\mathscr{T}_n(\mathbf{Q})$ is the nuclear kinetic-energy operator, and $\widetilde{\mathscr{H}_e}(\mathbf{r},\mathbf{Q})$ is the electronic Hamiltonian consisting of the nonrelativistic electronic Hamiltonian, $\mathscr{H}_e(\mathbf{r},\mathbf{Q})$, and the SO coupling, $\mathscr{H}_{\mathrm{SO}}(\mathbf{r},\mathbf{Q})$ (for details, see Sec. S1.1 in the Supporting Information). $\mathscr{H}_{\mathrm{SO}}(\mathbf{r},\mathbf{Q})$ is supposed to comprise the one-electron term, wherein the effect of the two-electron term is approximately included through the effective nuclear charge [45,46]. The explicit consideration of the two-electron term may be important for a molecule with large SO coupling, such as one having d elements. A vibronic Schrödinger equation is given by

$$[\mathscr{H}(\mathbf{r},\mathbf{Q}) - E_t]\Phi(\mathbf{r},\mathbf{Q}) = 0, \tag{3}$$

where $\Phi(\mathbf{r},\mathbf{Q})$ is the vibronic wavefunction and E_t is the total energy of a molecule. A usual approach to solve the above equation is expanding the vibronic wavefunction in terms of the electronic basis, of which types determine the matrix element of the vibronic Hamiltonian. The mixed-spin CA basis is employed in this study.

The Herzberg–Teller expansion of $\widetilde{\mathscr{H}_e}(\mathbf{r},\mathbf{Q})$ around reference nuclear configuration $\mathbf{Q} = \mathbf{0}$ is given by

$$\widetilde{\mathscr{H}_e}(\mathbf{r},\mathbf{Q}) = \widetilde{\mathscr{H}_e}(\mathbf{r},\mathbf{0}) + \widetilde{\mathscr{H}_e'}(\mathbf{r},\mathbf{Q}), \tag{4}$$

$$\widetilde{\mathscr{H}_e'}(\mathbf{r},\mathbf{Q}) = \sum_\alpha \left(\frac{\partial \widetilde{\mathscr{H}_e}(\mathbf{r},\mathbf{Q})}{\partial Q_{\alpha\overline{\Gamma}}}\right)_{\mathbf{0}} Q_{\alpha\overline{\Gamma}} + \frac{1}{2}\sum_{\alpha,\beta}\left(\frac{\partial^2 \widetilde{\mathscr{H}_e}(\mathbf{r},\mathbf{Q})}{\partial Q_{\alpha\overline{\Gamma}}\partial Q_{\beta\overline{\Gamma}'}}\right)_{\mathbf{0}} Q_{\alpha\overline{\Gamma}}Q_{\beta\overline{\Gamma}'} + \cdots. \tag{5}$$

Vibrational mode α is expressed with its irrep $\overline{\Gamma}$ of point group G. The electronic Schrödinger equation for $\widetilde{\mathscr{H}_e}(\mathbf{r},\mathbf{0})$ is given by

$$[\widetilde{\mathscr{H}_e}(\mathbf{r},\mathbf{0}) - E_{M\Gamma}(\mathbf{0})]\widetilde{\Psi}_{M\Gamma}(\mathbf{r},\mathbf{0}) = 0, \tag{6}$$

where $\{\widetilde{\Psi}_{M\Gamma}(\mathbf{r},\mathbf{0})\}$ is the mixed-spin CA basis and $E_{M\Gamma}(\mathbf{0})$ is the electronic energy of the mixed-spin state. Γ represents the irrep of the electronic wavefunction that includes spatial and spin parts. Note that the electronic Hamiltonian at $\mathbf{Q}=\mathbf{0}$ is expressed as

$$\widetilde{\mathscr{H}_e}(\mathbf{r},\mathbf{0}) = \mathscr{H}_e(\mathbf{r},\mathbf{0}) + \mathscr{H}_{\mathrm{SO}}(\mathbf{r},\mathbf{0}). \tag{7}$$

The electronic Schrödinger equation for the nonrelativistic electronic Hamiltonian $\mathbf{Q}=\mathbf{0}$, $\mathscr{H}_e(\mathbf{r},\mathbf{0})$, is given by

$$[\mathscr{H}_e(\mathbf{r},\mathbf{0}) - E_{k\Gamma}(\mathbf{0})]\Psi_{k\Gamma}(\mathbf{r},\mathbf{0}) = 0, \tag{8}$$

where $\{\widetilde{\Psi}_{k\Gamma}(\mathbf{r},\mathbf{0})\}$ is the pure-spin CA basis and $E_{k\Gamma}$ is the electronic energy of the pure-spin state. In the following, capital letters, M and N, and small letters, k, ℓ, m, and n, distinguish the different mixed-spin and pure-spin states, respectively. Both the mixed- and pure-spin CA bases are clamped at $\mathbf{Q}=\mathbf{0}$. In contrast, sets of eigenfunctions for $\mathscr{H}_e(\mathbf{r},\mathbf{Q})$ and $\widetilde{\mathscr{H}_e}(\mathbf{r},\mathbf{Q})$, called the pure-spin and mixed-spin BO bases, explicitly depend on the nuclear coordinates[12,17]. In the mixed-spin CA representation, a vibronic wavefunction is expanded using the mixed-spin CA basis,

$$\Phi(\mathbf{r},\mathbf{Q}) = \sum_M \chi_{Mv}(\mathbf{Q})\widetilde{\Psi}_{M\Gamma}(\mathbf{r},\mathbf{0}), \tag{9}$$

where $\chi_{Mv}(\mathbf{Q})$ is the vibrational wavefunction with $v=(v_1,\cdots,v_\alpha,\cdots,v_{3M-5\text{ or }3M-6})$ a set of vibrational quantum numbers. The vibrational Schrödinger equation in this representation is given by

$$\begin{aligned}\left[\mathscr{T}_n(\mathbf{Q}) + E_{M\Gamma}(\mathbf{0}) + \langle\widetilde{\Psi}_{M\Gamma}|\widetilde{\mathscr{H}_e'}(\mathbf{r},\mathbf{Q})|\widetilde{\Psi}_{M\Gamma}\rangle - E_t\right]\chi_{Mv}(\mathbf{Q}) \\ + \sum_{N\neq M}\langle\widetilde{\Psi}_{N\Gamma'}|\widetilde{\mathscr{H}_e'}(\mathbf{r},\mathbf{Q})|\widetilde{\Psi}_{M\Gamma}\rangle\,\chi_{Nv'}(\mathbf{Q}) = 0.\end{aligned} \tag{10}$$

This is the coupled differential equation.

The adiabatic approximation is employed to define an initial adiabatic state for the nonradiative transition. Within the mixed-spin CA adiabatic approximation, a vibronic wavefunction is given by

$$\Phi_{Mv}(\mathbf{r},\mathbf{Q}) = \chi_{Mv}(\mathbf{Q})\widetilde{\Psi}_{M\Gamma}(\mathbf{r},\mathbf{0}). \tag{11}$$

Then, $\chi_{Mv}(\mathbf{Q})$ is defined by the eigenfunction of the following vibrational Schrödinger equation;

$$\left[\mathscr{T}_n(\mathbf{Q}) + E_{M\Gamma}(\mathbf{0}) + \langle\widetilde{\Psi}_{M\Gamma}|\widetilde{\mathscr{H}_e'}(\mathbf{r},\mathbf{Q})|\widetilde{\Psi}_{M\Gamma}\rangle - E_{Mv}\right]\chi_{Mv}(\mathbf{Q}) = 0, \tag{12}$$

where $E_{M\nu}$ is the vibronic energy. The vibronic transitions from initial vibronic state $M\nu$ to final state $N\nu'$ are considered, treating the neglected coupling term as a perturbation. According to Fermi's golden rule, the nonradiative rate constant from initial mixed-spin state M to final state N is given by

$$k^{\mathrm{nr}}_{N\leftarrow M} = \frac{2\pi}{\hbar}\sum_{\nu,\nu'} P_{M\nu}(T)|(\mathbf{H})'_{NM}|^2\delta(E_{N\nu'} - E_{M\nu}), \tag{13}$$

$$(\mathbf{H})'_{NM} = \langle\chi_{N\nu'}|\,\langle\widetilde{\Psi}_{N\Gamma'}|\widetilde{\mathscr{H}'_e}(\mathbf{r},\mathbf{Q})|\widetilde{\Psi}_{M\Gamma}\rangle\,|\chi_{M\nu}\rangle\,. \tag{14}$$

Here, $P_{M\nu}(T)$ is the distribution of the initial vibrational states at temperature T, which is expressed as Boltzmann distribution in this study, assuming thermal equilibrium. Note that Eq. (11) cannot be used for degenerate systems, such as the dynamic Jahn–Teller system[47]. In this case, the potential part of the vibronic Hamiltonian must be diagonalized within the degenerate subspace to obtain the adiabatic states. Hence, electronic states are assumed to be non-degenerate below.

B. Vibronic Coupling Constant

In evaluating the nonradiative rate constant, the matrix element of $\widetilde{\mathscr{H}'_e}(\mathbf{r},\mathbf{Q})$ represented by the mixed spin CA basis (see Eqs. (12) and (14) for the diagonal and off-diagonal elements, respectively) needs to be calculated. From Eq. (5), the matrix element is given by

$$\langle\widetilde{\Psi}_{N\Gamma'}|\widetilde{\mathscr{H}'_e}(\mathbf{r},\mathbf{Q})|\widetilde{\Psi}_{M\Gamma}\rangle = \sum_{\alpha} V^{N\Gamma'M\Gamma}_{\alpha\bar{\Gamma}} Q_{\alpha\bar{\Gamma}} + \frac{1}{2}\sum_{\alpha,\beta} W^{N\Gamma'M\Gamma}_{\alpha\bar{\Gamma}\beta\bar{\Gamma}'} Q_{\alpha\bar{\Gamma}} Q_{\beta\bar{\Gamma}'} + \cdots, \tag{15}$$

where $V^{N\Gamma'M\Gamma}_{\alpha\bar{\Gamma}}$ and $W^{N\Gamma'M\Gamma}_{\alpha\bar{\Gamma}}$ are the linear and quadratic VCCs between mixed-spin states defined by

$$V^{N\Gamma'M\Gamma}_{\alpha\bar{\Gamma}} = \left\langle \widetilde{\Psi}_{N\Gamma'} \middle| \left(\frac{\partial\widetilde{\mathscr{H}_e}(\mathbf{r},\mathbf{Q})}{\partial Q_{\alpha\bar{\Gamma}}}\right)_{\mathbf{0}} \middle| \widetilde{\Psi}_{M\Gamma} \right\rangle, \tag{16}$$

$$W^{N\Gamma'M\Gamma}_{\alpha\bar{\Gamma}\beta\bar{\Gamma}'} = \left\langle \widetilde{\Psi}_{N\Gamma'} \middle| \left(\frac{\partial^2\widetilde{\mathscr{H}_e}(\mathbf{r},\mathbf{Q})}{\partial Q_{\alpha\bar{\Gamma}}\partial Q_{\beta\bar{\Gamma}'}}\right)_{\mathbf{0}} \middle| \widetilde{\Psi}_{M\Gamma} \right\rangle. \tag{17}$$

$V^{N\Gamma'M\Gamma}_{\alpha\bar{\Gamma}}$ is nonvanishing when the decomposition of the direct product $\Gamma'\times\Gamma$ contains $\bar{\Gamma}$ [48]. $V^{M\Gamma}_{\alpha\bar{\Gamma}} := V^{M\Gamma M\Gamma}_{\alpha\bar{\Gamma}}$ and $W^{M\Gamma}_{\alpha\bar{\Gamma}\beta\bar{\Gamma}'} := W^{M\Gamma M\Gamma}_{\alpha\bar{\Gamma}\beta\bar{\Gamma}'}$ represent the linear and quadratic diagonal VCCs, respectively. $V^{M\Gamma}_{\alpha\bar{\Gamma}}$ is nonvanishing when $\bar{\Gamma}$ is totally symmetric irrep in a non-degenerate electronic system [48].

The VCC between mixed-spin states can be expressed using the pure-spin basis. A mixed-spin state is written as a linear combination of pure-spin states,

$$|\widetilde{\Psi}_{M\Gamma}\rangle = \sum_k C_{kM} |\Psi_{k\Gamma}\rangle , \tag{18}$$

where C_{kM} is the mixing coefficient that depends on the SO coupling constant (SOCC) and electronic energy gap between pure-spin states. The pure-spin states with the same irreps are mixed. C_{kM} is determined by diagonalizing $\widetilde{\mathscr{H}_e}(\mathbf{r},\mathbf{0})$ represented by the pure-spin CA basis,

$$\langle \Psi_{\ell\Gamma'}|\widetilde{\mathscr{H}_e}(\mathbf{r},\mathbf{0})|\Psi_{k\Gamma}\rangle = \left(E_{k\Gamma}(\mathbf{0})\delta_{\ell k} + \lambda^{\ell\Gamma' k\Gamma}\right)\delta_{\Gamma'\Gamma}, \tag{19}$$

$$\lambda^{\ell\Gamma' k\Gamma} = \langle \Psi_{\ell\Gamma'}|\mathscr{H}_{\mathrm{SO}}(\mathbf{r},\mathbf{0})|\Psi_{k\Gamma}\rangle . \tag{20}$$

Here, $\lambda^{\ell\Gamma' k\Gamma}$ is the SOCC between pure-spin states at the reference nuclear configuration. This is nonvanishing when $\Gamma' \times \Gamma$ contains the totally symmetric irrep since $\mathscr{H}_{\mathrm{SO}}$ is totally symmetric[35]. Eq. (19) is block diagonalized concerning the irreps of pure-spin states. This method to variationally determine the mixing coefficients can be used even for degenerate and pseudo-degenerate cases and has broader applicability than the non-degenerate stationary perturbation theory [25].

From Eqs. (2), (16), and (18), the linear VCC between mixed-spin states is expressed as

$$V_{\alpha\overline{\Gamma}}^{N\Gamma' M\Gamma} = \sum_{k,\ell} C_{\ell N}^* C_{kM} \left(V_{\alpha\overline{\Gamma}}^{\ell\Gamma' k\Gamma} + \xi_{\alpha\overline{\Gamma}}^{\ell\Gamma' k\Gamma}\right), \tag{21}$$

where $V_{\alpha\overline{\Gamma}}^{\ell\Gamma' k\Gamma}$ is the linear VCC between pure-spin states,

$$V_{\alpha\overline{\Gamma}}^{\ell\Gamma' k\Gamma} = \left\langle \Psi_{\ell\Gamma'} \middle| \left(\frac{\partial \mathscr{H}_e(\mathbf{r},\mathbf{Q})}{\partial Q_{\alpha\overline{\Gamma}}}\right)_{\mathbf{0}} \middle| \Psi_{k\Gamma} \right\rangle . \tag{22}$$

Also, $\xi_{\alpha\overline{\Gamma}}^{\ell\Gamma' k\Gamma}$ is the first-order dependence of the SO coupling on the nuclear coordinates,

$$\xi_{\alpha\overline{\Gamma}}^{\ell\Gamma' k\Gamma} = \left\langle \Psi_{\ell\Gamma'} \middle| \left(\frac{\partial \mathscr{H}_{\mathrm{SO}}(\mathbf{r},\mathbf{Q})}{\partial Q_{\alpha\overline{\Gamma}}}\right)_{\mathbf{0}} \middle| \Psi_{k\Gamma} \right\rangle . \tag{23}$$

$V_{\alpha\overline{\Gamma}}^{\ell\Gamma' k\Gamma}$ and $\xi_{\alpha\overline{\Gamma}}^{\ell\Gamma' k\Gamma}$ are nonvanishing when the decomposition of the direct product $\Gamma' \times \Gamma$ contains $\overline{\Gamma}$[48]. $V_{\alpha\overline{\Gamma}}^{k\Gamma} := V_{\alpha\overline{\Gamma}}^{k\Gamma k\Gamma}$ represents the diagonal linear VCC of a pure-spin state. In a non-degenerate electronic system, $V_{\alpha\overline{\Gamma}}^{k\Gamma}$ is nonvanishing when $\overline{\Gamma}$ is totally symmetric irrep[48]. Thus, the selection rule of $V_{\alpha\overline{\alpha}}^{\ell\Gamma' k\Gamma}$ is the same as that of $V_{\alpha\overline{\alpha}}^{N\Gamma' M\Gamma}$. Similar expressions can be obtained for the quadratic VCC (Section S1.2).

The irrep of pure-spin state can be decomposed as that of spatial part Γ_1 and spin part Γ_2 using the representation of double group[35],

$$|\Psi_{k\Gamma}\rangle = |\Psi_k \Gamma_1, \Gamma_2\rangle . \tag{24}$$

This representation clarifies the transition channel based on the selection rule. For example, the selection rule of SOCC (Eq. (20)) can be separated into the spatial and spin parts; the SOCC is nonvanishing when the decomposition of $\Gamma_1' \times \Gamma_1$ and $\Gamma_2' \times \Gamma_2$ contains one of the irreps for the three-dimensional rotations to which the orbital and spin angular momentum operators belong (Section S1.3)[35]. Similarly, the linear VCC between pure-spin states (Eq. (22)) is nonvanishing when the decomposition of $\Gamma_1' \times \Gamma_1$ contains $\overline{\Gamma}$ as well as Γ_2' and Γ_2 are the same (Section S1.3). The VCC between pure-spin states with different spin multiplicities is vanishing because the vibronic coupling operator does not operate on the spin function[2].

C. Rate Constant of Intersystem Crossing

Thus far, the general expression for the nonradiative rate constant is described. Supposing that pure-spin states do not resonate by SO coupling, the nonradiative transition can be classified into IC and ISC based on the spin multiplicities of the large components in the initial and final mixed-spin states. Here, pure-spin states m and n are defined by the large components of initial and final mixed-spin states M and N, respectively, indicating that C_{mM} and C_{nN} are larger than the other mixing coefficients (c.f., Eq. (18)). The nonradiative transition when the spin multiplicities of pure-spin states m and n are the same is called the IC (Fig. 1 (a)). In contrast, the one with the different spin multiplicities of pure-spin states m and n is called the ISC. The IC rate constant without the SO coupling effect, i.e., $V_{\alpha\overline{\Gamma}}^{N\Gamma' M\Gamma} \approx V_{\alpha\overline{\Gamma}}^{n\Gamma' m\Gamma}$ (c.f., Eq. (21)), , was previously derived[26]. In the following, the ISC rate constant is obtained by using several approximations, assuming that the spin multiplicities of pure-spin states m and n are different.

The employed approximations are summarized as follows. (i) Only a linear off-diagonal vibronic coupling, which is responsible for the one-phonon process, is considered as a perturbation to induce the transition between mixed-spin states. In other words, the higher-order vibronic coupling that involves more than the one-phonon process is neglected. From this approximation, the ISC rate constant from initial mixed-spin state M to finial state N is given by

$$k_{N\leftarrow M}^{\mathrm{ISC}} = \sum_{\alpha,\beta} k_{N\leftarrow M,\alpha\beta}^{\mathrm{ISC}}, \tag{25}$$

$$k_{N\leftarrow M,\alpha\beta}^{\mathrm{ISC}} = \frac{2\pi}{\hbar} V_{\alpha\overline{\Gamma}}^{N\Gamma' M\Gamma} V_{\beta\overline{\Gamma}'}^{M\Gamma N\Gamma'} \Theta_{\alpha\overline{\Gamma}\beta\overline{\Gamma}'}, \tag{26}$$

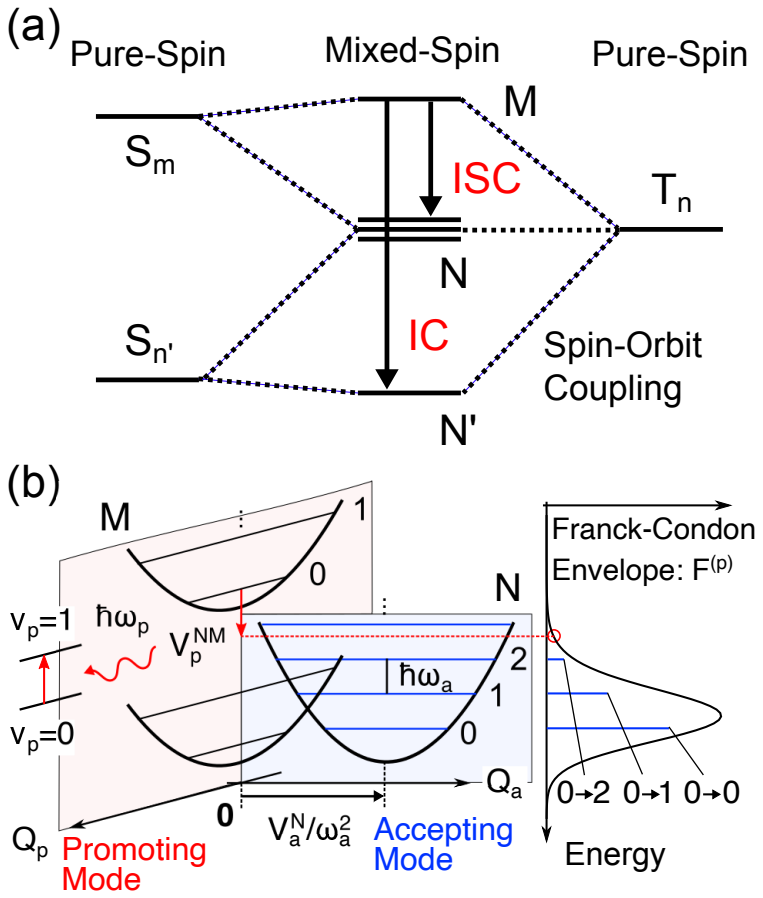

FIG. 1. (a) Classification of nonradiative transition into ISC and IC. (b) Schematic of nonradiative transition accompanied by one-phonon emission.

where $\Theta_{\alpha\bar{\Gamma}\beta\bar{\Gamma}'}$ is the nuclear part of the ISC rate constant defined by

$$\Theta_{\alpha\bar{\Gamma}\beta\bar{\Gamma}'} = \sum_{\nu,\nu'} P_{M\nu}(T)\,\langle\overline{\chi}_{N\nu'}|Q_{\alpha\bar{\Gamma}}|\chi_{M\nu}\rangle\,\langle\chi_{M\nu}|Q_{\beta\bar{\Gamma}'}|\overline{\chi}_{N\nu'}\rangle\,\delta(E_{N\nu'}-E_{M\nu}). \tag{27}$$

This is the density of the final vibronic states weighted by the nuclear moment factor. In Eq. (25), the ISC rate constant is decomposed by vibrational mode.

(ii) The vibrational wavefunction is approximated to the eigenfunction of the harmonic oscillator. This is valid when the Duschinsky rotation[49] and anharmonic effects on the potential energy surface are minor. (iii) The SO coupling effect on the diagonal VCC is neglected, i.e., $V_{\alpha\bar{\Gamma}}^{M\Gamma} \approx V_{\alpha\bar{\Gamma}}^{m\Gamma}$ and $V_{\alpha\bar{\Gamma}}^{N\Gamma'} \approx V_{\alpha\bar{\Gamma}}^{n\Gamma'}$, which is reasonable without the SO resonance of pure-spin states (Section S1.4). This approximation corresponds to replacing the vibrational wavefunctions for mixed-spin states M and N with the ones for pure-spin states m and n, respectively. Combining approximations (ii)

and (iii), the initial and final vibrational Schrödinger equations are written as

$$\left[E_{M\Gamma}(\mathbf{0})+\sum_{\alpha}\left(-\frac{\hbar^2}{2}\frac{\partial^2}{\partial Q_{\alpha\overline{\Gamma}}^2}+\frac{\omega_{\alpha\overline{\Gamma}}^2}{2}Q_{\alpha\overline{\Gamma}}^2\right)-E_{M\nu}\right]\chi_{M\nu}(\mathbf{Q})=0, \tag{28}$$

and

$$\left[E_{N\Gamma'}(\mathbf{0})+\sum_{\alpha}\left(-\frac{\hbar^2}{2}\frac{\partial^2}{\partial Q_{\alpha\overline{\Gamma}}^2}+V_{\alpha\overline{\Gamma}}^{n\Gamma'}Q_{\alpha\overline{\Gamma}}+\frac{\omega_{\alpha\overline{\Gamma}}^2}{2}Q_{\alpha\overline{\Gamma}}^2\right)-E_{N\nu'}\right]\overline{\chi}_{N\nu'}(\mathbf{Q})=0. \tag{29}$$

Note that, for simplicity, the reference nuclear configuration $\mathbf{Q}=\mathbf{0}$ is taken at the equilibrium geometry of pure-spin state m, resulting in $V_{\alpha\overline{\Gamma}}^{m\Gamma}=0$ because of the Hellmann–Feynman theorem[50,51]. The angular frequency $\omega_{\alpha\overline{\Gamma}}$ is obtained by diagonalizing the Hessian of pure-spin state m at $\mathbf{Q}=\mathbf{0}$. Final mixed-spin state N is displaced by $V_{\alpha\overline{\Gamma}}^{n\Gamma'}/\omega_{\alpha\overline{\Gamma}}^2$ along vibrational mode α with respect to initial state M, and the reorganization energy of final state N is given by $|V_{\alpha\overline{\Gamma}}^{n\Gamma'}|^2/2\omega_{\alpha\overline{\Gamma}}^2$ (Section S1.5). Detailed information on the potential energy surface is unnecessary in the CA representation because the CA basis does not explicitly depend on the nuclear coordinates; hence, the geometry optimization of the final electronic state is not required.

(iv) The dependence of the SO coupling on the nuclear coordinates (Eq. (23)) is neglected because this is considered to be smaller than vibronic coupling (Eq. (22))[8,15]. Then, the off-diagonal VCC between mixed-spin states is written as (Section S1.4)

$$V_{\alpha\overline{\Gamma}}^{N\Gamma'M\Gamma}=C_{nN}^{*}C_{nM}V_{\alpha\overline{\Gamma}}^{n\Gamma'}+\sum_{k\neq n}C_{nN}^{*}C_{kM}V_{\alpha\overline{\Gamma}}^{n\Gamma'k\Gamma}+\sum_{\ell\neq m}C_{\ell N}^{*}C_{mM}V_{\alpha\overline{\Gamma}}^{\ell\Gamma'm\Gamma}. \tag{30}$$

From Eqs. (21) to (30), C_{mM} and C_{nN}^{*} are supposed to be larger than the other coefficients, i.e., the product of the small mixing coefficients is neglected, and $V_{\alpha\overline{\Gamma}}^{m\Gamma}$ is set to 0 by taking $\mathbf{Q}=\mathbf{0}$ at the equilibrium geometry of pure-spin state m. The three terms in Eq. (30) have the same order. The first term corresponds to the direct transition in the pure-spin CA representation. The second and third terms correspond to the indirect transitions mediating pure-spin states k and ℓ, having the same spin multiplicities as n and m, respectively (Figs. S1, S2, and Table S2). The comparison in the transition matrix element between the mixed-spin and pure-spin CA representations is discussed in Section S1.6 based on the effective Hamiltonian approach[52,53], wherein the mixing coefficients are expressed using the non-degenerate stationary perturbation theory. The difference mainly appears in the direct transition term, which becomes the SOCC between electronic states m and n in the pure-spin CA representation and the diagonal VCC of pure-spin state n in the mixed-spin CA representation. In other words, the ISC rate constants within the mixed-spin and pure-spin CA approximations give similar numerical results when the direct SOCC is vanishing.

The selection rule of the ISC rate constant, which can be divided into that of the electronic and vibrational parts (Eq. (26)), is described. A vibrational mode that gives non-zero off-diagonal VCC between initial and final electronic states, $V_{\alpha\bar{\Gamma}}^{N\Gamma' M\Gamma}$, is called a promoting mode[54]. This mode is responsible for electronic transition through one-phonon emission and absorption. In contrast, a vibrational mode with non-zero diagonal VCC of final electronic state, $V_{\alpha\bar{\Gamma}}^{N\Gamma'}$ (approximated to $V_{\alpha\bar{\Gamma}}^{n\Gamma'}$ in this study), is called an accepting mode[54] because this mode, along which a potential energy surface is displaced, mainly accepts excess electronic energy. The promoting and accepting modes cannot be distinguished when the irreps of promoting and accepting modes are the same. The nuclear part, $\Theta_{\alpha\bar{\Gamma}\beta\bar{\Gamma}'}$, is nonvanishing when $\alpha=\beta$ or when both α and β are accepting modes [26]. Thus, the ISC rate constant, $k^{\mathrm{ISC}}_{N\leftarrow M,\alpha\beta}$, is nonvanishing when $\alpha=\beta$ with α being a promoting mode or when $\alpha\neq\beta$ with α and β being both promoting and accepting modes (that is, when promoting and accepting modes cannot be distinguished).

D. Nuclear Part of the Intersystem-Crossing Rate Constant

The nuclear part of the ISC rate constant is described. For tetracene, as discussed in Section 4.1, $k^{\mathrm{ISC}}_{N\leftarrow M,\alpha\beta}$ with $\alpha\neq\beta$ is vanishing because the promoting and accepting modes for the ISC can be distinguished according to the selection rule of vibronic coupling. Therefore, only the diagonal vibrational term is described below Omitting the irreps of electronic states and vibrational mode for simplicity, $\Theta_\alpha := \Theta_{\alpha\alpha}$ can be written as [26]

$$\Theta_\alpha = \sum_{\nu_\alpha} P_{m\nu_\alpha}(T)\left[\frac{(\nu_\alpha+1)\hbar}{2\omega_\alpha}F^{(\alpha)}(+\hbar\omega_\alpha)+\frac{\nu_\alpha\hbar}{2\omega_\alpha}F^{(\alpha)}(-\hbar\omega_\alpha)\right]. \tag{31}$$

Here, $F^{(\alpha)}(E)$ is the FC envelope excluding vibrational mode α,

$$F^{(\alpha)}(E)=\sum_{\nu\not\ni\nu_\alpha}\sum_{\nu'\not\ni\nu'_\alpha}\prod_{\gamma\neq\alpha}|\langle\bar{\nu}'_\gamma|\nu_\gamma\rangle|^2\delta(E_N-E_M+\sum_{\gamma\neq\alpha}\hbar\omega_\gamma(\nu'_\gamma-\nu_\gamma)+E), \tag{32}$$

where $|\nu_\gamma\rangle$ and $|\bar{\nu}'_\gamma\rangle$ are the initial and final single-mode vibrational states, respectively, and E_N-E_M is the electronic energy gap (Eqs. (S21) and (S22)). The multi-mode vibrational state, $|\chi_{M\nu}\rangle$, is expressed as a product of the single-mode vibrational states, $|\nu_\gamma\rangle$, without the Duschinsky rotation effect. Eq. (31) can be understood as an analogy to photon emission and absorption[55,56]. The first term in Eq. (31) indicates that the ISC occurs at $E=+\hbar\omega_\alpha$ through the one-phonon emission with vibrational energy $\hbar\omega_\alpha$ (Fig. 1 (b)), whereas whereas the second term with $E=-\hbar\omega_\alpha$ indicates the one-phonon absorption [26]. The phonon emission and absorption processes are dominant when

a final state is energetically lower and higher than an initial state, respectively. An example of the latter cases is the reverse ISC from T_1 to S_1 utilized in thermally activated delayed fluorescence for organic light-emitting diodes[57]. The phonon absorption occurs when the initial vibrational excited states are populated, i.e., $v_\alpha \neq 0$, at a finite temperature. For the reverse ISC from T_1 to S_1, the indirect transition that mediates the triplets energetically higher than T_1 is important (Fig. S2 (c))[58,59].

The FC overlap integral between the displaced harmonic oscillators is given by[60,61]

$$\langle \overline{v}'_\gamma | v_\gamma \rangle = \sqrt{\frac{v_\gamma! v'_\gamma!}{2^{v_\gamma + v'_\gamma}}} e^{-\frac{|g^n_\gamma|^2}{4}} \sum_{l=0}^{\min[v_\gamma, v'_\gamma]} (-1)^{v_\gamma - l} 2^l \frac{|g^n_\gamma|^{v_\gamma + v'_\gamma - 2l}}{l!(v_\gamma - l)!(v'_\gamma - l)!}, \tag{33}$$

which depends on the dimensionless diagonal VCC defined by

$$g^n_\gamma = \frac{V^n_\gamma}{\sqrt{\hbar \omega^3_\gamma}}. \tag{34}$$

Note that $\langle \overline{v}'_\gamma | v_\gamma \rangle = \delta_{v'_\gamma, v_\gamma}$ when $g^n_\gamma = 0$, or when the final electronic state is not displaced with respect to the initial state. The accepting mode that gives nonzero g^n_γ contributes to broadening the FC envelope and, hence, receiving the excess electronic energy after the phonon emission and absorption.

The computational cost of the FC envelope in the energy representation (Eq. (32)) is high because the summation over many vibrational quantum numbers is necessary. This problem can be circumvented by the Fourier transformation of the FC envelope from the energy to time representations. The FC envelope in the time representation is given by [38,39]

$$F^{(\alpha)}(E) = \frac{1}{2\pi} \int_{-\infty}^{\infty} d\tau \, \rho^{(\alpha)}(\tau) e^{i(E_N - E_M + E)\tau}, \tag{35}$$

where τ is the time divided by $\hbar$ and $\rho^{(\alpha)}$ is the correlation function of vibrational states without including vibrational mode α. For displaced harmonic oscillators, $\rho^{(\alpha)}$ is given by [62],

$$\rho^{(\alpha)}(\tau) = \prod_{\gamma \neq \alpha} \rho_\gamma(\tau), \tag{36}$$

$$\rho_\gamma(\tau) = \exp\left(-\frac{|g^2_\gamma|^2}{2}(2n_\gamma + 1) + \frac{|g^n_\gamma|^2}{2}(n_\gamma + 1) e^{i\hbar\omega_\gamma \tau} + \frac{|g^n_\gamma|^2}{2} n_\gamma e^{-i\hbar\omega_\gamma \tau} \right), \tag{37}$$

where $n_\gamma = (e^{\hbar\omega_\gamma / k_B T} - 1)^{-1}$ (k_B is the Boltzmann constant) is the number of excited vibrations of mode γ in thermal equilibrium. $n_\gamma \to 0$ in the limit of $T \to 0$ K. In nature, the density of final

vibronic states is continuously broadened by neglected interactions, such as rovibronic interactions and interactions with the surrounding environment. This broadening can be approximately expressed using the Gaussian function with linewidth σ;

$$F^{(\alpha)}(E) = \frac{1}{2\pi}\int_{-\infty}^{\infty} d\tau\ \rho^{(\alpha)}(\tau)e^{-\sigma^2\tau^2/2}e^{i(E_N-E_M+E)\tau}. \tag{38}$$

The Gaussian function is usually employed to describe inhomogeneous broadening arising from various interactions with different strengths [2,38].

E. Vibronic Coupling Density

The irreps of electronic states and vibrational modes are omitted for simplicity. The VCD is given by an integrand of the VCC[27–29],

$$V_\alpha^{NM} = \int d\boldsymbol{x}\ \eta_\alpha^{NM}(\boldsymbol{x}), \tag{39}$$

where $\boldsymbol{x} = (x, y, z)$ is the three-dimensional Cartesian coordinate and

$$\eta_\alpha^{NM}(\boldsymbol{x}) = \begin{cases} \Delta\rho_{NM}(\boldsymbol{x}) \times v_\alpha(\boldsymbol{x}) & (N = M) \\ \rho_{NM}(\boldsymbol{x}) \times v_\alpha(\boldsymbol{x}) & (N \neq M) \end{cases}. \tag{40}$$

$\eta_\alpha^N(\boldsymbol{x}) := \eta_\alpha^{NN}(\boldsymbol{x})$ is the diagonal VCD and $\eta_\alpha^{NM}(\boldsymbol{x})$ with $N \neq M$ is the off-diagonal VCD. $\Delta\rho_{NM}(\boldsymbol{x})$ and $\rho_{NM}(\boldsymbol{x})$ are the electron density difference and overlap density between electronic states ℓ and k, respectively (Section S1.6). $v_\alpha(\boldsymbol{x})$ is the potential derivative of vibrational mode α. The VCD elucidates the local picture of vibronic coupling from electronic and vibrational structures separately.

III. METHOD OF CALCULATION

The ISC rate constant of tetracene was calculated using Eqs. (25) and (26), wherein the off-diagonal VCC was evaluated from Eq. (30) (the mixing coefficients are obtained by diagonalizing Eq. (19)) and the nuclear part from Eqs. (31), (36), (37), and (38). The Fourier transform in Eq. (38) was performed using FFTW3 [63]. Photoluminescence quantum efficiency (PLQY) was evaluated from the ISC, IC, and fluorescence rate constants (Section S1.7). The SOCC, VCC, and VCD were computed using in-house codes. The computational method for the SOCC was described in Ref. 64 and for the VCC and VCD were described in Refs. 29 and 44.

The ground and excited electronic structures of tetracene were calculated at the B3LYP/6-31G(d,p) and TD-B3LYP/6-31G(d,p) within the Tamm–Dancoff approximation, respectively, based on density functional theory (DFT). The solvent effect was included through the polarizable continuum model (PCM) [65]. B3LYP best reproduces the experimental energy difference of S_1–T_1 for tetracene [66,67] among B3LYP, M06-2X, and ωB97XD functionals (Table S3). Also, B3LYP reproduces well the lineshape and wavelength of the experimental fluorescence spectrum[66] (Fig. S3). These results indicate that this functional is suitable for the calculations of tetracene. A linewidth of the Gaussian function that reproduces the lineshape of the experimental fluorescence spectrum is 200 cm^{-1} (Table S4). This computational condition for the density of final vibronic states is used to calculate the fluorescence, IC, and ISC rate constants. The electronic and vibrational structures were computed using Gaussian 16 Revision C.01 [68].

IV. RESULTS

A. Rate Constant of Intersystem Crossing

The electronic structures of tetracene in cyclohexane solution were calculated. The geometry-optimized structure in the S_1 excited state was D_{2h} symmetry, which was confirmed to be stable by vibrational analysis. The irreps of the spin functions in D_{2h} symmetry are given by (Tables S5 and S6)

$$E_{1/2,g} \otimes E_{1/2,g} = \{A_g\} \oplus B_{1g} \oplus B_{2g} \oplus B_{3g}, \tag{41}$$

where $\{\ \}$ represents the antisymmetric product. A table of Clebsch–Gordan coefficients [69,70] shows that the spin-singlet belongs to $\Gamma_2 = A_g$, whereas the spin-triplet belongs to $\Gamma_2 = B_{1g}$, B_{2g}, and B_{3g}. The spin-triplet with B_{1g} irrep is of the spin projection 0. The linear combination of the spin triplets with the B_{2g} and B_{3g} irreps gives those of the spin projections ± 1.

Figure 2 (a) shows the energy levels of pure-spin states at the S_1 optimized structure. The spin-singlets from S_1 to S_3 and spin-triplets from T_1 to T_5 are considered as a model space to obtain the mixed-spin states. The nonvanishing SOCCs are for S_1-T_3 (0.52 cm^{-1}), S_1-T_4 (1.41 cm^{-1}), and S_3-T_1 (1.36 cm^{-1}) in the x component of the angular momentum operator (Table S7). Table I summarizes the irreps of the pure-spin states The pure-spin states with the same irreps Γ are mixed by the SO coupling. Specifically, S_1, T_3, and T_4 constitute the mixed-spin states with the B_{1u} irrep, and S_3 and T_1 constitute the mixed-spin states with the B_{2u} irrep.

Figure 2 (b) shows the energy levels of the mixed-spin states, which can be classified into those whose large components are spin-singlet and spin-triplet since the pure-spin states do not resonate by the SO coupling (see Table S8 for the mixing coefficients).

TABLE I. Irreps of pure-spin state Γ, and its spatial part Γ_1 and spin part Γ_2. Γ is obtained by the direct product of Γ_1 and Γ_2.

	Γ	Γ_1	Γ_2		Γ	Γ_1	Γ_2		Γ	Γ_1	Γ_2
S_1	B_{1u}	B_{1u}	A_g	T_2	B_{2g}	B_{3g}	B_{1g}	T_4	B_{3u}	B_{2u}	B_{1g}
S_2	B_{3g}	B_{3g}	A_g		B_{1g}	B_{3g}	B_{2g}		A_u	B_{2u}	B_{2g}
S_3	B_{2u}	B_{2u}	A_g		A_g	B_{3g}	B_{3g}		B_{1u}	B_{2u}	B_{3g}
T_1	A_u	B_{1u}	B_{1g}	T_3	B_{3u}	B_{2u}	B_{1g}	T_5	B_{2g}	B_{3g}	B_{1g}
	B_{3u}	B_{1u}	B_{2g}		A_u	B_{2u}	B_{2g}		B_{1g}	B_{3g}	B_{2g}
	B_{2u}	B_{1u}	B_{3g}		B_{1u}	B_{2u}	B_{3g}		A_g	B_{3g}	B_{3g}

The ISC from the mixed-spin state $4B_{1u}$, whose large component is S_1, to the energetically close mixed-spin state $5A_g$, which is equal to T_2 because of no mixing with the spin-singlets, was calculated. The mixed-spin states $4B_{1u}$ and $5A_g$ are written as

$$|\widetilde{\Psi}_{4B_{1u}}\rangle = C_{S_1}|\Psi_{S_1B_{1u}}\rangle + C_{T_3}|\Psi_{T_3B_{1u}}\rangle + C_{T_4}|\Psi_{T_4B_{1u}}\rangle, \tag{42}$$

$$|\widetilde{\Psi}_{5A_g}\rangle = |\Psi_{T_2A_g}\rangle, \tag{43}$$

where $C_{S_1} \approx 1.00$, $C_{T_3} \approx -8.80 \times 10^{-5}i$, and $C_{T_4} \approx -1.93 \times 10^{-4}i$ (Table S8) represent the mixing coefficients of S_1, T_3, and T_4 in $4B_{1u}$, respectively. The ISC from $4B_{1u}$ to $6B_{1g}$ ($|\widetilde{\Psi}_{6B_{1g}}\rangle = |\Psi_{T_2},B_{1g}\rangle$) and $7B_{2g}$ ($|\widetilde{\Psi}_{7B_{2g}}\rangle = |\Psi_{T_2},B_{2g}\rangle$), which are degenerate with $5A_g$, are symmetry-forbidden, as discussed below. In addition, the ISC from $4B_{1u}$ to the mixed-spin states whose large components are T_1, T_3, T_4, and T_5 are $< 10^0$ s^{-1}. Table II shows the calculated ISC rate constant from $4B_{1u}$ to $5A_g$ as well as the IC and fluorescence rate constants from S_1 to S_0 at $T = 300$ K. The computational results reproduce the experimental rate constants and PLQY well[40]. The calculated IC rate constant is small because of the large energy gap between S_1 and S_0 (2.55 eV), as predicted by the experiments[1]. Although in Table II the linewidth of the Gaussian function is set to 200 cm^{-1}, which reproduces the lineshape of the fluorescence spectrum, the dependence of the rate constants on the Gaussian function is not strong (Table S9).

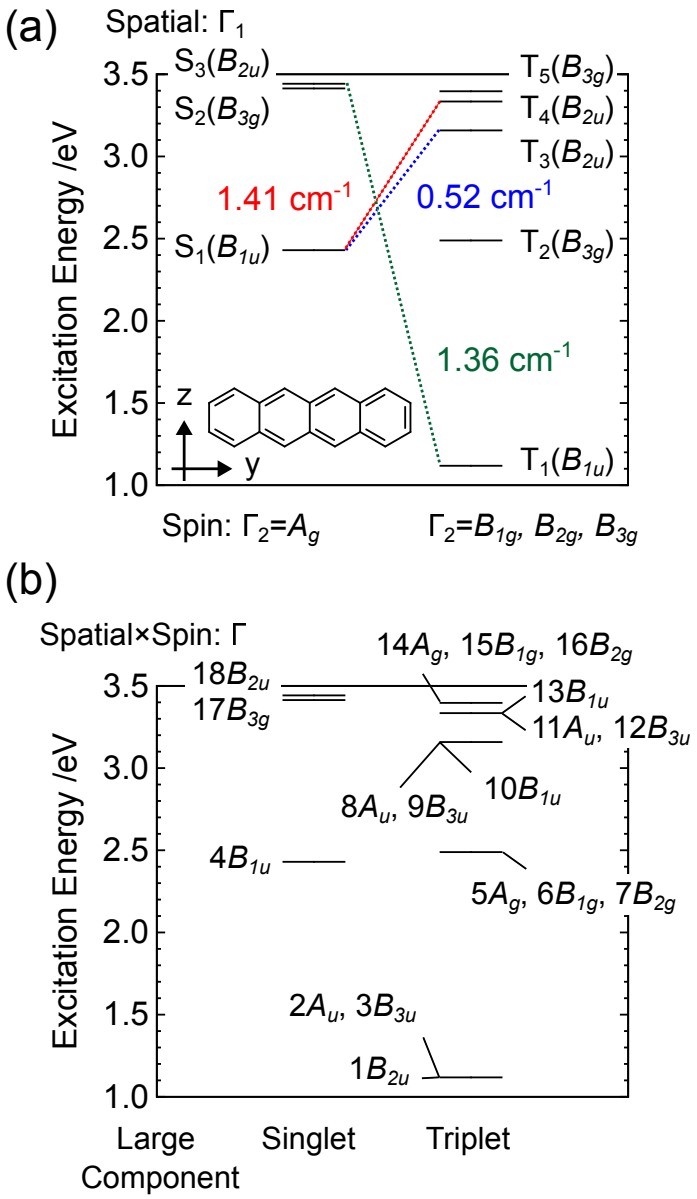

FIG. 2. (a) Energy levels of pure-spin states at the S_1 optimized structure. Irreps of the spatial part Γ_1 are given in parenthesis. The absolute values of the nonvanishing SOCCs between spin-singlets and -triplets are written. (b) Energy levels of mixed-spin states with their irreps Γ. The left and right columns are the mixed-spin states whose large component is the spin-singlets and spin-triplets, respectively.

The contributing factors to the ISC rate constant from initial mixed-spin state $4B_{1u}$ to final state $5A_g$ are examined from its vibrational-mode decomposition. The reducible representation of the vibrational modes of tetracene in D_{2h} symmetry is decomposed as follows:

$$\Gamma_{\mathrm{vib}}(D_{2h}) = 15A_g + 6B_{1g} + 7B_{2g} + 14B_{3g} + 7A_u + 14B_{1u} + 14B_{2u} + 7B_{3u}. \tag{44}$$

TABLE II. Calculated rate constants of fluorescence and IC from S_1 to S_0, rate constant of ISC from $4B_{1u}$ to $5A_g$, and PLQY for tetracene in cyclohexane at $T = 300$ K. The density of final vibronic states is expressed using the Gaussian function with a linewidth of 200 cm^{-1}.

	k^{f} /s^{-1}	k^{IC} /s^{-1}	k^{ISC} /s^{-1}	Φ
Calc.	3.13×10^7	5.59×10^2	9.44×10^7	0.25
Exp.[40]	3.49×10^7		8.55×10^7	0.29

The off-diagonal VCC between mixed-spin states $4B_{1u}$ and $5A_g$ is nonvanishing when the irrep of the vibrational mode is B_{1u}; the promoting mode belongs to B_{1u} irrep. The diagonal VCC of $5A_g$ is nonvanishing when the irrep of the vibrational mode is A_g; the accepting mode belongs to A_g irrep. Since the irreps of the promoting and accepting modes are different, the vibrational cross-term ($\alpha \neq \beta$) of the ISC rate constant is vanishing. Thus, the vibrational diagonal term, i.e., $k^{\mathrm{ISC}}_{N\leftarrow M,\alpha} := k^{\mathrm{ISC}}_{N\leftarrow M,\alpha\alpha}$, is considered in the following.

The off-diagonal VCC based on the mixed-spin basis is expressed using the pure-spin basis. From Eqs. (42) and (43), the off-diagonal VCC between $4B_{1u}$ and $5A_g$ is given by

$$V^{5A_g 4B_{1u}}_{\alpha B_{1u}} = C_{\mathrm{T}_3} V^{\mathrm{T}_2 A_g \mathrm{T}_3 B_{1u}}_{\alpha B_{1u}} + C_{\mathrm{T}_4} V^{\mathrm{T}_2 A_g \mathrm{T}_4 B_{1u}}_{\alpha B_{1u}}, \tag{45}$$

which comprises the linear combination of the off-diagonal VCCs between T_3 and T_2 as well as T_4 and T_2. This corresponds to the indirect transition from S_1 to T_2 mediating T_3 and T_4 in the pure-spin representation. $V^{\mathrm{T}_2 A_g \mathrm{T}_3 B_{1u}}_{\alpha B_{1u}}$ and $V^{\mathrm{T}_2 A_g \mathrm{T}_4 B_{1u}}_{\alpha B_{1u}}$ in Eq. (45) are nonvanishing because the irrep of the spin part of $|\Psi_{\mathrm{T}_2 A_g}\rangle$ is the same as that of $|\Psi_{\mathrm{T}_3 B_{1u}}\rangle$ and $|\Psi_{\mathrm{T}_4 B_{1u}}\rangle$, i.e., $\Gamma_2 = B_{3g}$ (Table I). The off-diagonal VCCs between $4B_{1u}$ and $6B_{1g}/7B_{2g}$ are vanishing from the selection rule of the spin part, which results in forbidding the ISC from $4B_{1u}$ to $6B_{1g}$ and $7B_{2g}$.

Figures 3 (a)–(c) show the rate constant and its electronic and nuclear parts for the ISC from $4B_{1u}$ to $5A_g$ plotted with respect to vibrational modes (Eq. (26)). The numbering of the vibrational modes is in the ascending order of the frequency. The promoting modes that give the largest and second-largest contributions to the ISC rate constant are modes 4 and 20, respectively. In particular, the ISC promoted by mode 4 is dominant because of the large nuclear part. The reason is understood from the FC envelope without promoting mode 4, $F^{(4)}(E)$ (Fig. 3 (d)) (Eq. (38)). The excess excitation energy after the phonon emission and absorption of promoting mode 4 is accepted by the FC envelope at $E = +\hbar\omega_4$ and $E = -\hbar\omega_4$, respectively (Eq. (31)). The FC factor

of the 0–0 transition, of which position corresponds to the energy gap between $4B_{1u}$ and $5A_g$, is located at $E = +5.9$ meV. Since the energy gap is small, the excess excitation energy is mainly accepted by the final vibrational ground state characterized by the 0–0 peak of the FC factor. The accepting modes, such as modes 9 and 62 with the large dimensionless diagonal VCCs (Fig. S4), contribute less to accepting the excitation energy in the present case. Note that the FC envelope drastically decreases with respect to the energy. Therefore, the increase of the phonon emission and absorption energies of the promoting mode leads to a small nuclear part (see Fig. S5 for the FC envelope without promoting mode 20).

The FC envelope without promoting mode 4 has a larger value at $E = +\hbar\omega_4$ than $E = -\hbar\omega_4$ (Fig. 3 (d)), indicating that the ISC mainly proceeds through the phonon emission. In particular, the phonon emission with $\nu_4 = 0$, which corresponds to the spontaneous emission in the photon case, is a major process (Table S10). Nevertheless, the phonon emission and absorption with $\nu_4 \geq 1$ also occurs because the vibrationally excited states of mode 4 with a small frequency of 161 cm^{-1} are populated to some extent at $T = 300$ K. In contrast, the phonon absorption of promoting mode 20 does not much occur because of the large frequency, $\omega_{20} = 620$ cm^{-1} (Table S10).

Figure S6 shows the ISC rate constant plotted by changing the energy gap between S_1 and T_2 while fixing the other parameters. The ISC rate constant drastically decreases with the increase of the energy gap. This behavior reflects the lineshape of the FC envelope that decays exponentially concerning the energy gap, i.e., the energy gap law [6]. The upper limit of the rate constant is determined by the maximum value of the FC envelope that depends on the FC factors and energy gap.

B. Vibronic Coupling Density Analysis

It was found that vibrational mode 4 is the primary promoting mode for the ISC from $4B_{1u}$ to $5A_g$. The overlap density between $4B_{1u}$ and $5A_g$ is given by

$$\rho_{5A_g 4B_{1u}} = C_{\mathrm{T}_3}\rho_{\mathrm{T}_2\mathrm{T}_3} + C_{\mathrm{T}_4}\rho_{\mathrm{T}_2\mathrm{T}_4}, \tag{46}$$

where $\rho_{\mathrm{T}_2\mathrm{T}_3}$ and $\rho_{\mathrm{T}_2\mathrm{T}_4}$ are the overlap densities between T_3 and T_2 as well as T_4 and T_2, respectively. T_2 mainly comprises the HOMO-1–LUMO and HOMO–LUMO+1 transitions, whereas T_3 comprises the HOMO-2–LUMO transition and T_4 the HOMO–LUMO+2 transition (Table S11). Hence, the overlap density between T_3 and T_2 can be approximately expressed as the HOMO-2–

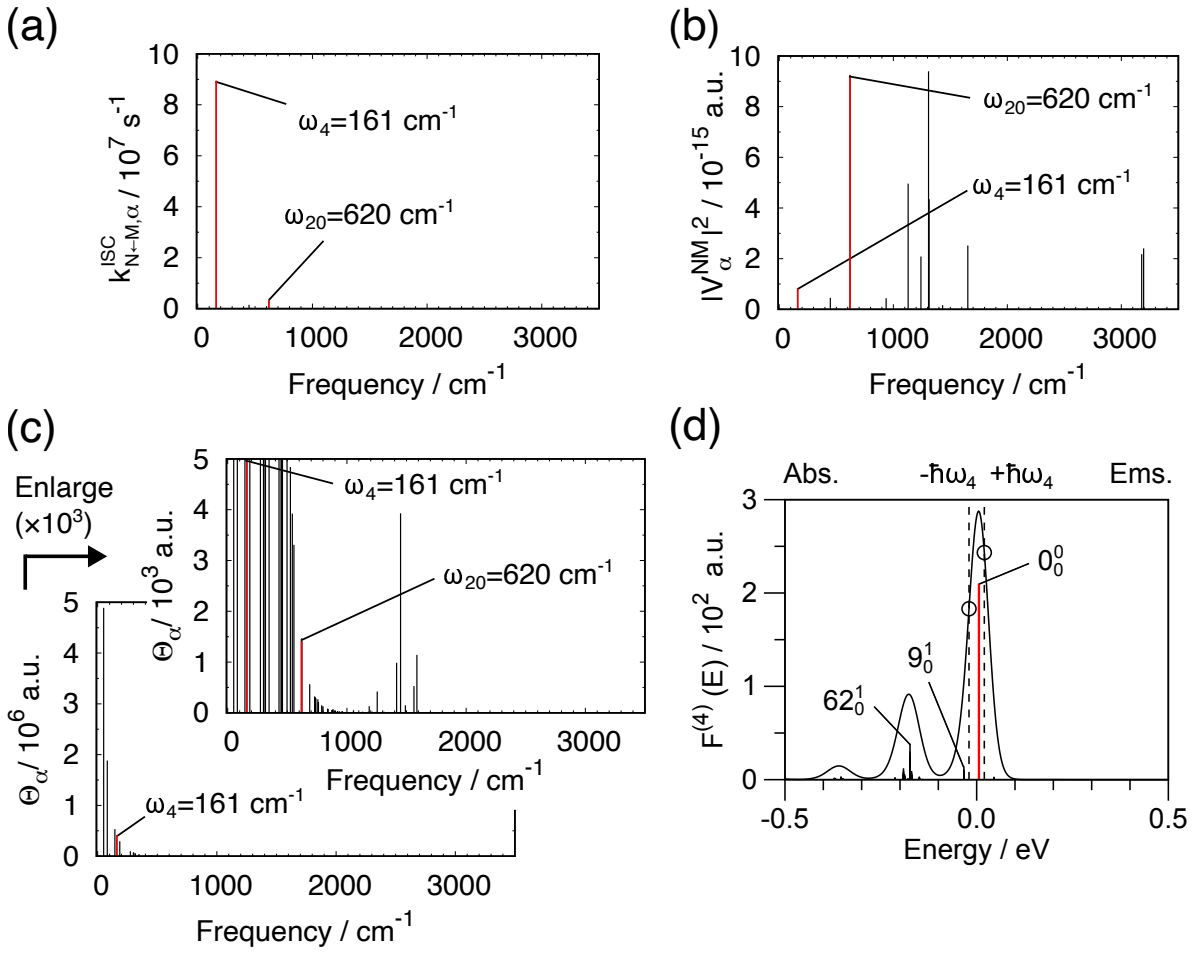

FIG. 3. (a) Rate constant, $k^{\mathrm{ISC}}_{N\leftarrow M,\alpha}$, and its (b) electronic part, $|V^{N\Gamma' M\Gamma}_{\alpha\overline{\Gamma}}|^2$ and (c) vibrational part, $\Theta_{\alpha\overline{\Gamma}}$, for the ISC from initial mixed-spin state $4B_{1u}$ to final state $5A_g$ plotted with respect to vibrational modes. $V^{N\Gamma' M\Gamma}_{\alpha\overline{\Gamma}}$ is nonvanishing when $\overline{\Gamma} = B_{1u}$. $\Theta_{\alpha\overline{\Gamma}}$ is nonvanishing no matter $\overline{\Gamma}$ is. The primary promoting modes are modes 4 and 20. (d) FC factors (vertical line) and envelope without ipromoting mode 4. 0^0_0 represents the FC factor of the 0-0 transition. 9^0_1 and 62^0_1 represent the FC factors between the initial vibrational quantum number 0 and final number 1 for the accepting modes 9 and 62, respectively.

HOMO product and the one between T_4 and T_2 as the LUMO+1–LUMO+2 product (the molecular orbitals are shown in Fig. S7). Figure 4 shows the results of the off-diagonal VCD analysis (Eq. (40)) between T_4 and T_2 at the S_1 optimized structure. The overlap density has a large distribution on C2 (and its symmetric counterpart C3, C8, C9) as well as C5a (and its symmetric counterpart C11a), which couples strongly with the potential derivative of mode 4 with C2–C3 and C5a–C11a vibrations. Consequently, the off-diagonal VCD is localized on C2 and C5a, indicating that the off-diagonal VCC between T_4 and T_2 originates from these sites. Introducing

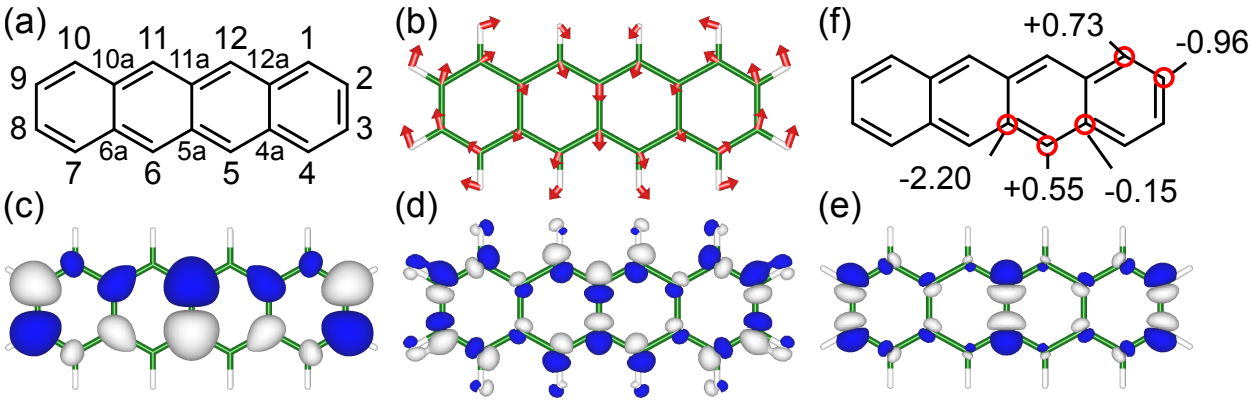

FIG. 4. (a) Atomic labels of tetracene, (b) vibrational mode 4, (c) overlap density between T_4 and T_2, ρ_{nm}, (d) potential derivative of mode 4, v_α, (e) off-diagonal VCD, $\eta_{nm,\alpha}$, and (f) atomic decomposition of the off-diagonal VCC in 10^{-4} a.u. Isosurface values of (c), (d), and (e) are 1×10^{-3}, 5×10^{-3}, and 5×10^{-6} a.u., respectively.

substituents on C2, C3, C8, and C9 that withdraw the overlap densities on these sites is expected to reduce the off-diagonal VCC values.

V. CONCLUSIONS

We derived an analytical expression for the nonradiative rate constant based on Fermi's golden rule within the mixed-spin CA approximation, wherein the nonradiative transition is regarded as vibronically-induced phonon emission and absorption processes between mixed-spin states, or the eigenstates of the electronic Hamiltonian that contains the SO coupling. The vibrational modes are classified into the promoting and accepting modes, which are responsible for the phonon emission/absorption and accepting excess excitation energy after the phonon emission/absorption, respectively, according to the selection rule of vibronic coupling. The ease of accepting the excitation energy is governed by the FC envelope that depends on the FC factors and energy gap between initial and final states. The mixed-spin CA representation provides a unified treatment of the photophysical processes, i.e., IC, ISC, fluorescence, and phosphorescence, aside from the differences in the driving force (vibronic coupling or electron-photon coupling) and spin multiplicity change for the transition. The ISC rate constants within the mixed-spin and pure-spin CA approximations give similar numerical results when the direct SOCC between initial and final pure-spin states is vanishing.

The obtained expression was applied to tetracene. The calculated ISC rate constant from the mixed-spin state whose large component is S_1 to the one whose large component is T_2 reproduces the experimental result well. The primary promoting mode for the ISC process is mode 4 with a frequency of 161 cm^{-1}. The excess excitation energy after the phonon emission and absorption of mode 4 is mainly accepted by the final vibrational ground state. The off-diagonal VCC of mode 4 originates from the center and edge C atoms of tetracene. Thus, based on the quantitative calculation of the rate constant, we identified the important vibrational mode for ISC and clarified the origin of the vibronic coupling of that mode, which can be applied to rational molecular design with the controlled ISC process.

ACKNOWLEDGMENTS

This study was supported by JSPS KAKENHI Grant Number JP22H02157 in Scientific Research (B), and JP22K05253 in Scientific Research (C). Numerical calculations were partly performed at Supercomputer System, Institute for Chemical Research, Kyoto University, Academic Center for Computing and Media Studies (ACCMS), Kyoto University, the information initiative center, Hokkaido University, and Research Center for Computational Science, Okazaki (Project: 22-IMS-C065).

REFERENCES

[1]N. J. Turro, V. Ramamurthy, V. Ramamurthy, and J. C. Scaiano, *Principles of Molecular Photochemistry: An Introduction* (University Science Books, Sausalito, CA, 2009).

[2]E. S. Medvedev and V. I. Osherov, *Radiationless Transitions in Polyatomic Molecules* (Springer-Verlag, New York, 1995).

[3]G. Fischer, *Vibronic Coupling: The Interaction between the Electronic and Nuclear Motions* (Academic Press, London, 1984).

[4]T. Azumi and K. Matsuzaki, “What does the term "vibronic coupling" mean?” Photochem. Photobiol. **25**, 315 (1977).

[5]M. Bixon and J. Jortner, “Intramolecular radiationless transitions,” J. Chem. Phys. **48**, 715–726 (1968).

[6]R. Englman and J. Jortner, "The energy gap law for radiationless transitions in large molecules," Mol. Phys. **18**, 145–164 (1970).

[7]W. Siebrand, "Mechanisms of intersystem crossing in aromatic hydrocarbons," Chem. Phys. Lett. **6**, 192 (1970).

[8]B. R. Henry and W. Siebrand, "Spin–orbit coupling in aromatic hydrocarbons. analysis of nonradiative transitions between singlet and triplet states in benzene and naphthalene," J. Chem. Phys. **54**, 1072 (1971).

[9]V. Lawetz, G. Orlandi, and W. Siebrand, "Theory of intersystem crossing in aromatic hydrocarbons," J. Chem. Phys. **56**, 4058–4072 (1972).

[10]G. Orlandi and W. Siebrand, "Basis-independent matrix elements for radiationless transitions and their application to intersystem crossing," Chem. Phys. Lett. **21**, 217 (1973).

[11]T. Azumi, "Reinterpretation of the non-fluorescent properties of the n, π^* singlet state," Chem. Phys. Lett. **17**, 211 (1972).

[12]T. Azumi, "Choice of basis functions in the theoretical treatments of intersystem crossing, proposal of a new selection rule," Chem. Phys. Lett. **25**, 135 (1974).

[13]B. Sharf and R. Silbey, "On the effect of deuteration on non-radiative processes in large molecules," Chem. Phys. Lett. **5**, 314–316 (1970).

[14]B. Sharf, "Intersystem-crossing brocesses in aromatic molecules," Chem. Phys. Lett. **14**, 475 (1972).

[15]A. C. Albrecht, "Vibronic—spin-orbit perturbations and the assignment of the lowest triplet state of benzene," J. Chem. Phys. **38**, 354–365 (1963).

[16]B. Sharf, "Introducing the extended born–oppenheimer representation for describing spin forbidden radiative and non-radiative transitions," Chem. Phys. Lett. **19**, 35 (1973).

[17]N. Shimakura, Y. Fujimura, and T. Nakajima, "Choice of basis sets for intersystem crossing," Chem. Phys. Lett. **40**, 222 (1976).

[18]Q. Peng, Y. Niu, Q. Shi, X. Gao, and Z. Shuai, "Correlation function formalism for triplet excited state decay: Combined spin–orbit and nonadiabatic couplings," J. Chem. Theory Comput. **9**, 1132 (2013).

[19]M. Etinski, J. Tatchen, and C. M. Marian, "Time-dependent approaches for the calculation of intersystem crossing rates," J. Chem. Phys. **134**, 154105 (2011).

[20]M. Etinski, V. Rai-Constapel, and C. M. Marian, "Time-dependent approach to spin-vibronic coupling: Implementation and assessment," J. Chem. Phys. **140**, 114104 (2014).

[21]I. Kim, S. O. Jeon, D. Jeong, H. Choi, W.-J. Son, D. Kim, Y. M. Rhee, and H. S. Lee, "Spin–vibronic model for quantitative prediction of reverse intersystem crossing rate in thermally activated delayed fluorescence systems," J. Chem. Theory Comput. **16**, 621 (2020).

[22]T. J. Penfold, E. Gindensperger, C. Daniel, and C. M. Marian, "Spin-vibronic mechanism for intersystem crossing," Chem. Rev. **118**, 6975 (2018).

[23]S. K. Lower and M. A. El-Sayed, "The triplet state and molecular electronic processes in organic molecules," Chem. Rev. **66**, 199–241 (1966).

[24]G. Baryshnikov, B. Minaev, and H. Ågren, "Theory and calculation of the phosphorescence phenomenon," Chem. Rev. **117**, 6500 (2017).

[25]B. de Souza, G. Farias, F. Neese, and R. Izsák, "Predicting phosphorescence rates of light organic molecules using time-dependent density functional theory and the path integral approach to dynamics," J. Chem. Theory Comput. **15**, 1896 (2019).

[26]W. Ota, M. Uejima, and T. Sato, "Role of vibronic couplings and energy gap in the internal conversion process of a molecule," Bull. Chem. Soc. Jpn. **96**, 582 (2023).

[27]T. Kato, N. Haruta, and T. Sato, *Vibronic Coupling Density: Understanding Molecular Deformation* (Springer, Singapore, 2021).

[28]T. Sato, K. Tokunaga, and K. Tanaka, "Vibronic coupling in naphthalene anion: Vibronic coupling density analysis for totally symmetric vibrational modes," J. Phys. Chem. A **112**, 758 (2008).

[29]M. Uejima, T. Sato, D. Yokoyama, K. Tanaka, and J.-W. Park, "Quantum yield in blue-emitting anthracene derivatives: Vibronic coupling density and transition dipole moment density," Phys. Chem. Chem. Phys. **16**, 14244 (2014).

[30]M. Uejima, T. Sato, M. Detani, A. Wakamiya, F. Suzuki, H. Suzuki, T. Fukushima, K. Tanaka, Y. Murata, C. Adachi, and H. Kaji, "A designed fluorescent anthracene derivative: Theory, calculation, synthesis, and characterization," Chem. Phys. Lett. **602**, 80 (2014).

[31]W. Ota, K. Takahashi, K. Higashiguchi, K. Matsuda, and T. Sato, "Origin of aggregation-induced enhanced emission: Role of pseudo-degenerate dlectronic states of excimers formed in aggregation phases," J. Mater. Chem. C **8**, 8036 (2020).

[32]S. Kimura, M. Uejima, W. Ota, T. Sato, S. Kusaka, R. Matsuda, H. Nishihara, and T. Kusamoto, "An open-shell, luminescent, two-dimensional coordination polymer with a honeycomb lattice and triangular organic radical," J. Am. Chem. Soc. **143**, 4329 (2021).

[33]Y. Hattori, R. Kitajima, W. Ota, R. Matsuoka, T. Kusamoto, T. Sato, and K. Uchida, "The

simplest structure of a stable radical showing high fluorescence efficiency in solution: Benzene donors with triarylmethyl radicals," Chem. Sci. **13**, 13418 (2022).

[34]T. Inui, Y. Tanabe, and Y. Onodera, *Group Theory and Its Applications in Physics*, Vol. 78 (Springer-Verlag, Berlin, 1990).

[35]A. J. Ceulemans, *Group Theory Applied to Chemistry* (Springer, Dordrecht, 2013).

[36]T. Sato and A. Ceulemans, "Vibronic and spin-orbit coupling of a d^9 transition-metal ion encapsulated in an icosahedral cage: The $(\Gamma_8+\Gamma_9)\times(g+2h)$ Jahn–Teller problem," J. Chem. Phys. **126**, 184501 (2007).

[37]T. Sato, E. Lijnen, and A. Ceulemans, "Jahn–Teller instability of icosahedral $[W@Au_{12}]^-$," J. Chem. Theory Comput. **10**, 613–622 (2014).

[38]G. C. Schatz and M. A. Ratner, *Quantum Mechanics in Chemistry* (Dover Publications, New York, 2002).

[39]A. Nitzan, *Chemical Dynamics in Condensed Phases: Relaxation, Transfer and Reactions in Condensed Molecular Systems* (Oxford university press, 2006).

[40]N. Nijegorodov, V. Ramachandran, and D. Winkoun, "The dependence of the absorption and fluorescence parameters, the intersystem crossing and internal conversion rate constants on the number of rings in polyacene molecules," Spectrochim. Acta, Part A **53**, 1813–1824 (1997).

[41]C. Burgdorff, T. Kircher, and H.-G. Löhmannsröben, "Photophysical properties of tetracene derivatives in solution," Spectrochim. Acta, Part A **44**, 1137–1141 (1988).

[42]Y. F. Pedash, O. Prezhdo, S. Kotelevskiy, and V. Prezhdo, "Spin–orbit coupling and luminescence characteristics of conjugated organic molecules. i. polyacenes," J. Mol. Struct. **585**, 49–59 (2002).

[43]A. Manian and S. P. Russo, "The dominant nature of Herzberg–Teller berms in the photophysical description of naphthalene compared to anthracene and tetracene," Sci. Rep. **12**, 21481 (2022).

[44]T. Sato, K. Tokunaga, N. Iwahara, K. Shizu, and K. Tanaka, "Vibronic coupling constant and vibronic coupling density," in *The Jahn-Teller Effect: Fundamentals and Implications for Physics and Chemistry*, edited by H. Köppel, D. R. Yarkony, and H. Barentzen (Springer-Verlag, Berlin and Hidelberg, 2009) pp. 99–129.

[45]S. Koseki, M. S. Gordon, M. W. Schmidt, and N. Matsunaga, "Main group effective nuclear charges for spin-orbit calculations," J. Phys. Chem. **99**, 12764–12772 (1995).

[46]D. G. Fedorov, S. Koseki, M. W. Schmidt, and M. S. Gordon, "Spin-orbit coupling in molecules: Chemistry beyond the adiabatic approximation," Int. Rev. Phys. Chem. **22**, 551–592 (2003).

[47]T. Sato, L. F. Chibotaru, and A. Ceulemans, "The $E \otimes e$ dynamic Jahn–Teller problem: A new insight from the strong coupling limit," J. Chem. Phys. **122**, 054104 (2005).

[48]I. B. Bersuker and V. Z. Polinger, *Vibronic Interactions in Molecules and Crystals* (Springer-Verlag, Berlin, 1989).

[49]F. Duschinsky, "On the interpretation of electronic spectra of polyatomic molecules," Acta Physicochim. URSS **7**, 551 (1937).

[50]H. Hellmann, *Einführung in die Quantenchemie* (Deuticke and Company, Leipzog, 1937).

[51]R. P. Feynman, "Forces in molecules," Physical review **56**, 340 (1939).

[52]C. E. Soliverez, "An effective hamiltonian and time-independent perturbation theory," J. Phys. C: Solid St. Phys. **2**, 2161–2174 (1969).

[53]I. Lindgren, "The Rayleigh–Schrodinger perturbation and the linked-diagram theorem for a multi-configurational model space," J. Phys. B: At. Mol. Phys. **7**, 2441 (1974).

[54]S.-H. Lin and R. Bersohn, "Effect of partial deuteration and temperature on triplet-state lifetimes," The Journal of Chemical Physics **48**, 2732–2736 (1968).

[55]J. J. Sakurai, *Advanced Quantum Mechanics* (Addison-Wesley, Reading, MA, 1967).

[56]D. P. Craig and T. Thirunamachandran, *Molecular Quantum Electrodynamics: An Introduction to Radiation-Molecule Interactions* (Dover Publications, New York, 1998).

[57]H. Uoyama, K. Goushi, K. Shizu, H. Nomura, and C. Adachi, "Highly efficient organic light-emitting diodes from delayed fluorescence," Nature **492**, 234–238 (2012).

[58]J. Gibson, A. P. Monkman, and T. J. Penfold, "The importance of vibronic coupling for efficient reverse intersystem crossing in thermally activated delayed fluorescence molecules," ChemPhysChem **17**, 2956–2961 (2016).

[59]M. K. Etherington, J. Gibson, H. F. Higginbotham, T. J. Penfold, and A. P. Monkman, "Revealing the spin–vibronic coupling mechanism of thermally activated delayed fluorescence," Nat. Commun. **7**, 13680 (2016).

[60]E. Hutchisson, "Band spectra intensities for symmetrical diatomic molecules," Phys. Rev. **36**, 410 (1930).

[61]A. Palma and J. Morales, "Franck–condon factors and ladder operators. i. harmonic oscillator," Int. J. Quantum Chem. **24**, 393 (1983).

[62]R. Kubo and Y. Toyozawa, "Application of the method of generating function to radiative and non-radiative transitions of a trapped electron in a crystal," Prog. Theor. Phys. **13**, 160 (1955).

[63]M. Frigo and S. G. Johnson, "The design and implementation of FFTW3," Proc. IEEE **93**, 216

(2005).

[64]T. Sato, M. Uejima, K. Tanaka, H. Kaji, and C. Adachi, "A light-emitting mechanism for organic light-emitting diodes: Molecular design for inverted singlet–triplet structure and symmetry-controlled thermally activated delayed fluorescence," J. Mater. Chem. C **3**, 870–878 (2015).

[65]J. Tomasi, B. Mennucci, and R. Cammi, "Quantum mechanical continuum solvation models," Chem. Rev. **105**, 2999 (2005).

[66]M. Taniguchi and J. S. Lindsey, "Database of absorption and fluorescence spectra of $>$ 300 common compounds for use in photochem CAD," Photochem. Photobiol. **94**, 290–327 (2018).

[67]A. Völcker, H.-J. Adick, R. Schmidt, and H.-D. Brauer, "Near-infrared phosphorescence emission of compounds with low-lying triplet states," Chem. Phys. Lett. **159**, 103–108 (1989).

[68]M. J. Frisch, G. W. Trucks, H. B. Schlegel, G. E. Scuseria, M. A. Robb, J. R. Cheeseman, G. Scalmani, V. Barone, G. A. Petersson, H. Nakatsuji, X. Li, M. Caricato, A. V. Marenich, J. Bloino, B. G. Janesko, R. Gomperts, B. Mennucci, H. P. Hratchian, J. V. Ortiz, A. F. Izmaylov, J. L. Sonnenberg, D. Williams-Young, F. Ding, F. Lipparini, F. Egidi, J. Goings, B. Peng, A. Petrone, T. Henderson, D. Ranasinghe, V. G. Zakrzewski, J. Gao, N. Rega, G. Zheng, W. Liang, M. Hada, M. Ehara, K. Toyota, R. Fukuda, J. Hasegawa, M. Ishida, T. Nakajima, Y. Honda, O. Kitao, H. Nakai, T. Vreven, K. Throssell, J. A. Montgomery Jr., J. E. Peralta, F. Ogliaro, B. Bearpark, H. J. J, E. Brothers, K. N. Kudin, V. N. Staroverov, T. Keith, R. Kobayashi, J. Normand, K. Raghavachari, A. Rendell, J. C. Burant, S. S. Iyengar, J. Tomasi, M. Cossi, J. M. Millam, M. Klene, C. Adamo, R. Cammi, J. W. Ochterski, R. L. Martin, K. Morokuma, O. Farkas, J. B. Foresman, and D. J. Fox, Gaussian 16, Revision C. 01, Gaussian, Inc., Wallingford, CT (2019).

[69]S. L. Altmann and P. Herzig, *Point-Group Theory Tables* (Clarendon, Oxford, 1994).

[70]G. F. Koster, J. O. Dimmock, R. G. Wheeler, and H. Statz, *Properties of the Thirty-Two Point Groups*, Vol. 24 (MIT press, Cambridge, MA, 1963).